

CrystEngComm

Accepted Manuscript



This is an *Accepted Manuscript*, which has been through the Royal Society of Chemistry peer review process and has been accepted for publication.

Accepted Manuscripts are published online shortly after acceptance, before technical editing, formatting and proof reading. Using this free service, authors can make their results available to the community, in citable form, before we publish the edited article. We will replace this *Accepted Manuscript* with the edited and formatted *Advance Article* as soon as it is available.

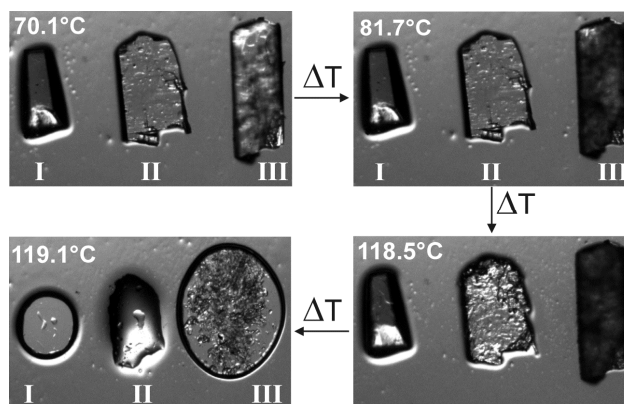
You can find more information about *Accepted Manuscripts* in the [Information for Authors](#).

Please note that technical editing may introduce minor changes to the text and/or graphics, which may alter content. The journal's standard [Terms & Conditions](#) and the [Ethical guidelines](#) still apply. In no event shall the Royal Society of Chemistry be held responsible for any errors or omissions in this *Accepted Manuscript* or any consequences arising from the use of any information it contains.

Figure for the table of contents

Investigations on the Trimorphism of *N*-(3-pyridyl)-benzamide

Christian Näther, Inke Jess, Julia Bahrenburg, Dennis Bank and Friedrich Temps



5 Three polymorphic modifications of *N*-(3-pyridyl)-benzamide were structurally characterized and investigated for their transition behavior and thermodynamic relations.

Cite this: DOI: 10.1039/c0xx00000x

www.rsc.org/xxxxxx

PAPER

Trimorphism of *N*-(3-Pyridyl)-Benzamide

Christian Näther^{[a]*}, Inke Jess^[a], Julia Bahrenburg^[b], Dennis Bank^[b] and Friedrich Temps^[b]*Received (in XXX, XXX) Xth XXXXXXXXXX 2011, Accepted Xth XXXXXXXXXX 2011*

DOI: 10.1039/b000000x

Three polymorphic modifications of *N*-(3-pyridyl)-benzamide (Form **I**, monoclinic, space group $P2_1/c$, $Z = 4$, form **II**, monoclinic, space group $P2_1$, $Z = 4$ and form **III**, monoclinic, space group $C2/c$, $Z = 8$) were obtained and characterized by single crystal X-ray diffraction. In all forms significant differences in the torsion of the phenyl rings and the arrangement of the molecules in the crystal are observed. Quantum chemical calculations of the conformational barriers reveal only small differences and indicate that the conformation of form **III** is energetically favoured but this form does not represent the minimum energy conformation. In the crystal structures of all forms the molecules are connected *via* intermolecular N-H \cdots N (form **I**) and N-H \cdots O (form **II** and **III**) hydrogen bonds into chains. Solvent mediated conversion and DSC experiments indicate that form **I** represents the thermodynamically stable form between -20°C and its melting point. Solidification of the melt or sublimation leads directly to form **I** or to an amorphous material that transforms into form **I** on crystallization. Form **II** and form **III** cannot be obtained as phase-pure materials. Mixtures of form **I** and **II** with form **II** as the minor component can be obtained sometimes by crystallization under kinetic control. Upon heating these mixtures, form **II** transforms into form **I** in an endothermic reaction, which indicates that both modifications are enantiotropically related with form **II** being stable at lower temperatures. Thermomicroscopic investigations on selected single crystals of form **III** show a polymorphic transition presumably to form **I** because melting is observed at exactly the same temperature as measured for **I**.

Introduction

The present study was performed as a part of a project on the investigation of the ultrafast dynamics of the bistable ESIPT (excited state intramolecular proton transfer) switch *N*-(3-pyridinyl)-2-pyridinecarboxamide (NPPCA). ESIPT switches offer two huge advantages compared to other photoswitchable molecules. In the first place, photoinduced proton transfer reactions belong to the fastest chemical processes known. Reaction times have been found down to $\tau = 20\text{--}100$ fs.^[1-2] Secondly, due to their exceptional photostabilities, ESIPT molecules allow for record numbers of reproducible, repeatable switching cycles. Well-known examples are the ESIPT compounds used in commercial sunscreens which protect us against skin cancer caused by harmful UV-A and UV-B light. Our investigations have shown that the intramolecular proton transfer process in NPPCA probably occurs within less than 500 fs.^[3] To support this conclusion, we decided to perform a study on the ultrafast dynamics of the closely related molecule *N*-(3-pyridyl)-benzamide where the proton donating nitrogen is replaced by a carbon and the intramolecular proton transfer cannot take place. In this context the exact structure of this molecule was of special interest and therefore this compound was investigated by single crystal X-ray diffraction.

Within these investigations we accidentally obtained crystals of two different polymorphic modifications (form **II** and form **III**) by recrystallization from ethyl acetate. We also found that after some days these crystals transform into a third modification

(form **I**). Even if the occurrence of different crystalline modifications is a widespread phenomenon that is of importance in academic and industrial research,^[4-10] trimorphic systems are relatively rare. Some examples are given in the reference list.^[11-24] In all three modifications of the investigated system significant differences in the torsion angles are found, which is called conformational polymorphism.^[25] To obtain insight into the rotational barriers and the stability of the different modifications quantum chemical calculations and investigations using differential scanning calorimetry (DSC), thermomicroscopy, X-ray powder diffraction (XRPD) and crystallization experiments were performed.

Results and Discussion

Crystal Growth

When the compound is crystallized from ethyl acetate a mixture of single crystals of different morphology is obtained that corresponds to two different polymorphic modifications (Figure S1 in the electronic supplementary information (ESI)). Form **II** consists of plate-like crystals, whereas blocks are observed for form **III** (Figure 1 and Figure S1 in the ESI). Storing this batch with the rest of mother liquid for about two days at room temperature leads to the formation of a new form (**I**) that show a significantly different morphology (Figure 1 and Figure S1 in the ESI). Subsequent X-ray powder diffraction (XRPD) measurements of the crystalline batch and a comparison of these results with the patterns calculated for

each form from the single crystal data show that all crystals of forms **II** and **III** have transformed to form **I** (Figure S2 in the ESI). This observation proves that this modification represents the thermodynamic stable form at room temperature. It has to be noted that several other batches obtained by recrystallization from ethyl acetate have been investigated but all of them consist only of form **I**. This observation is not unusual because in cases, where the surrounding is contaminated by crystals of the thermodynamically stable phase, the metastable crystals are difficult to prepare or cannot be obtained at all.^[26] The images in Figure 1 were obtained from crystals of the first batch, from which some crystals were transferred into an inert oil for the structure determinations. Under these conditions the crystals of the different modifications are stable.

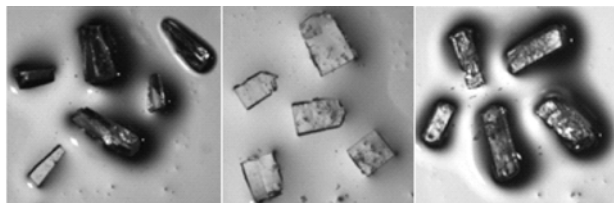


Figure 1. Microscopic images of form **I** (left), **II** (mid) and **III** (right).

Crystal Structures

Form **I** crystallizes in the centrosymmetric space group $P2_1/c$ with $Z = 4$ and one molecule in a general position. The central C7-C1-N1-C2 fragment is nearly planar with a torsion angle of $-175.9(2)^\circ$ (Table 1). The pyridine ring is practically coplanar to this fragment, whereas the benzene ring is rotated out of this plane by $24.5(1)^\circ$ (Figure 2 and Table 1). The dihedral angle between the pyridine and the benzene ring is about $24.3(1)^\circ$ (Table 1) and the pyridine N atom is located on the same side as the carbonyl O atom (Figure 2).

Form **II** crystallizes in the non-centrosymmetric space group $P2_1$ with $Z = 4$ and two crystallographically independent molecules in the asymmetric unit. The overall conformation in both molecules is very similar with comparable torsion and dihedral angles but the N atoms of the pyridyl ring (N2 and N22) point in opposite directions, which clearly proves that both molecules are different (Figure 2 and Table 1). In contrast to form **I** the pyridine ring is rotated out of the C7-C1-N1-C2 plane by $35.0(4)^\circ$ and $34.8(4)^\circ$ and the dihedral angle between the pyridine and the benzene ring amounts to $64.2(2)$ and $62.8(2)^\circ$, respectively (Table 1). Therefore the overall conformation is clearly different from that in form **I**.

Form **III** crystallizes in the centrosymmetric space group $C2/c$ with $Z = 8$ and all atoms in general positions. The central C7-C1-N1-C2 fragment is nearly planar with a torsion angle of $-176.5(2)^\circ$ (Figure 2 and Table 1). The pyridine ring is rotated out of this plane by $33.0(1)^\circ$, whereas the benzene ring is rotated by $30.6(2)^\circ$ in the opposite direction (Table 1). The dihedral angle between the pyridine and the benzene ring is about $63.3(1)^\circ$, thus the conformation is comparable to those of form **II** (Table 1).

In the crystal structure of form **I** the molecules are linked *via* N-H...N hydrogen bonds between the N-H hydrogen atom and the pyridine N atom. This leads to the formation of chains that elongate in the direction of the crystallographic *c*-axis (Figure

3: top). The N-H...N angle of 165.3° indicates that these hydrogen bonds are relatively strong (Table 2). Along these chains the C=O groups are always located on different sites of the chains leading to a zig-zag-like arrangement.

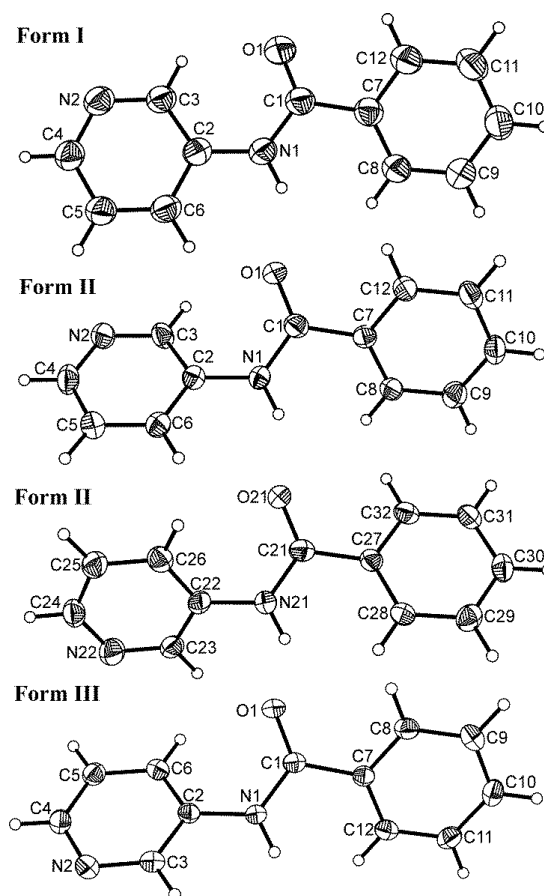


Figure 2. View of the asymmetric units in the crystal structures of form **I**, **II** and **III** with labeling and displacement ellipsoids drawn at the 50% probability level. Please note that the structure of form **II** contains two crystallographically independent molecules, denoted as a (top) and b (bottom).

Table 1. Torsion and dihedral angles ($^\circ$) in form **I**, **II** and **III**. Please note that C7-C1-N1-C2 is equivalent to C27-C21-N21-C22. Plane 1 refer to the pyridine, plane 2 to the benzene ring.

Form	I	II	II	III
C7-C1-N1-C2	$-175.9(2)$	$-179.0(4)$	$-178.4(4)$	$-176.5(2)$
Plane 1 / Plane 2	$2.3(1)$	$35.0(4)$	$34.8(4)$	$33.0(1)$
Plane 1 / Plane 3	$24.5(1)$	$29.4(4)$	$28.0(4)$	$30.6(2)$
Plane 1 / Plane 3	$24.3(1)$	$64.2(2)$	$62.8(2)$	$63.3(1)$

In contrast, in form **II** intermolecular N-H...O hydrogen bonding between the amide H atom and the carbonyl oxygen atom is observed leading to chains that elongate along the crystallographic *a*-axis (Figure 3: middle and Table 2). These chains are arranged in layers and within each layer the N-H vector of neighboring chains points in opposite directions (Figure 3: middle).

In the crystal structure of form **III** the molecules are also connected *via* N-H...O hydrogen bonds. This leads to the formation of chains that elongate in the direction of the crystallographic *b*-axis (Figure 3: bottom and Table 2). The N-H...O angle of 158.61° is slightly larger than in form **II** indicating that this is a relatively strong interaction. Neighboring chains are nearly coplanar and are arranged into

Cite this: DOI: 10.1039/c0xx00000x

www.rsc.org/xxxxxx

layers parallel to the *a-b*-plane (Figure 3: bottom). In contrast to form **II** the N-H vector of neighboring chains within each layer always points in the same direction.

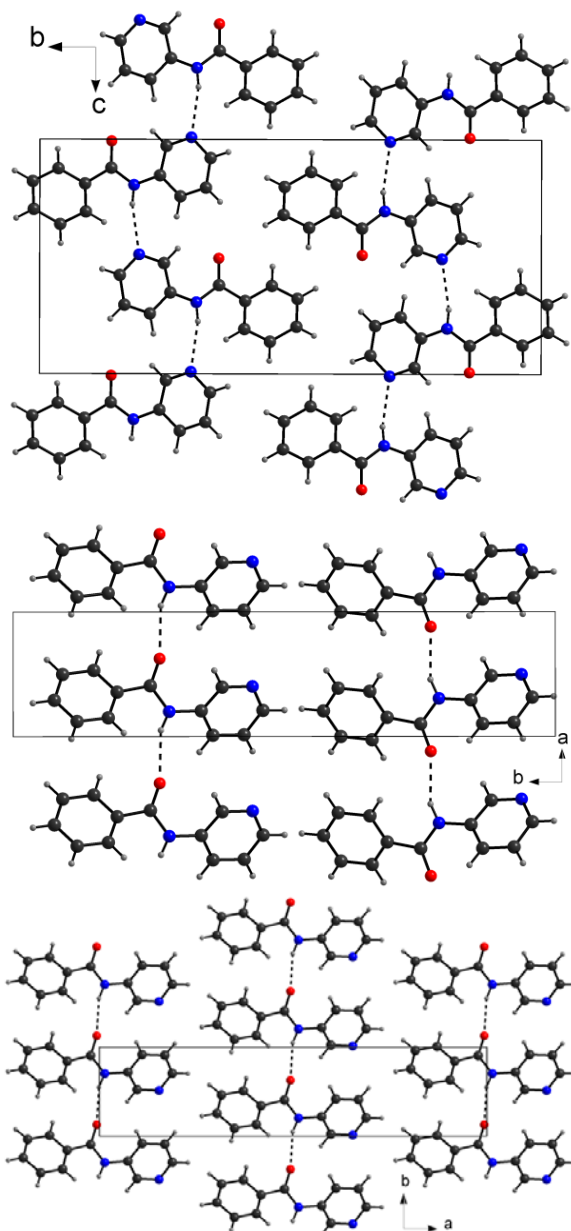


Figure 3. Crystal structures of form **I** (top), **II** (mid) and **III** (bottom) with intermolecular hydrogen bonding shown as dashed lines.

Large structural differences are also observed in the arrangement of the hydrogen bonded chains (Figure 4). In form **I** the neighboring molecules are rotated by 180° within each chain and the chains are closely packed in a way that the benzene rings of one chains fit perfectly into the apertures formed by the benzene rings of the neighboring chains

indicating $\pi \cdots \pi$ interactions between the respective benzene moieties (Figure 4: top).

Table 2. Bond lengths (Å) and angles (°) between the hydrogen bonded units in form **I**, **II** and **III**. Symmetry codes for the generation of equivalent atoms: D #*x*, -*y*+3/2, *z*+1/2, B = { . 4/#/#)/#/# # { . 4/#/# }/#D = *x*, *y*-1, *z*.

Form	D-H	d(H..A)	<DHA	d(D..A)
I	N1-H1...N2A	2.320	3.176 (29)	165.3
II	N1-H1...O1B	51574	61383#8,	48519###
II	N21-H21...O21C	51567	61389#9,	48817###
III	N1-H1...O1D	2.213	3.050 (2)	158.6

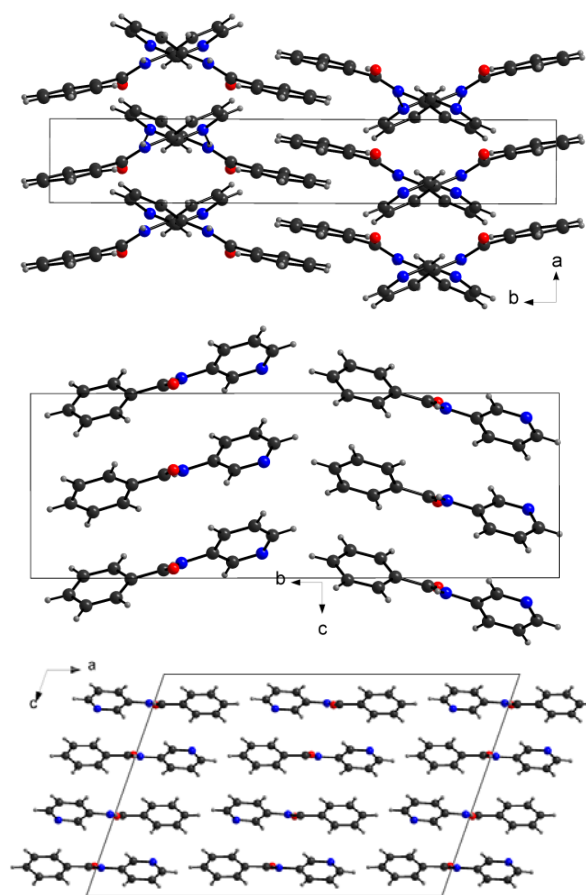


Figure 4. Crystal structures of form **I** (top), **II** (middle) and **III** (bottom).

In contrast to form **I**, in form **II** and **III** all molecules along the chains show the same orientation (Figure 4: mid and bottom). In form **III** the neighboring chains are always coplanar to each other, whereas in form **II** they form a herringbone arrangement. Moreover, in form **II** all pyridine rings point in the same direction of the crystallographic *b*-axis, which nicely demonstrates the non-centrosymmetric arrangement of the molecules.

Quantum chemical calculations of the conformational energy differences

To gain some information on the differences in conformation energy between the molecules in all forms, quantum chemical calculations at the B3LYP/6-311++G(d,p) level of theory at 298.15 K were performed starting from the crystallographic structures determined at low temperatures. The relative energies between the different structures ($\Delta(\Delta H)$) are given in Table 3. In order to prevent torsional motion, the torsion angles along the C-N-C-C fragment were fixed, whereas all other structural parameters were optimized. Additionally a total optimization was performed to determine the minimum energy conformation.

Table 3. Energy differences $\Delta(\Delta H)$ between the molecules in form **I**, **II** and **III**. Please note that the structure of form **II** contain to crystallographically independent molecules, denoted as a and b.

Form	$\Delta(\Delta H / \text{kJ/mol})$
I	-1.1
IIa	3
IIb	071:
III	-4.9
Fully optimized	-7.7

These calculations indicate that the conformation observed in molecule **a** of form **II** is the highest in energy, followed by that in form **I** which is more stable by only about 1.1 kJ/mol (Table 3). The molecule in form **III** is the lowest in energy followed by molecule **b** of form **II**. The difference between these forms is only about 0.2 kJ/mol. A total optimization of these four structures proves that none of them corresponds to the structure in the energetic minimum, which is 7.7 kJ/mol more stable than molecule **a** in form **II**. The fact that the conformation observed in form **I** is not the lowest in energy is not in contradiction to our results where this form represents the thermodynamically stable form at room temperature. Such small energies can be easily overcompensated by the packing energy of the crystal.

Investigations on the preparation and the transition behavior of all forms

The crystallization experiments mentioned above clearly show that at room temperature form **II** and form **III** transform into form **I**. Therefore the latter represents the thermodynamically stable form at room temperature.

Investigations of form **I** by means of differential scanning calorimetry (DSC) measurements show melting at an onset temperature (T_o) of 115.8°C (Figure 5). On cooling crystallization takes place at significant lower temperatures ($T_o = 54.1^\circ\text{C}$). The heat of fusion was determined from several DSC runs and is about 22.5 kJ/mol (Table S1 in the ESI). There are no hints for any polymorphic transition before melting, indicating that form **I** is also thermodynamically stable up to the melting point. It has to be noted that the heat of crystallization ΔH_c is significantly lower than that the heat of fusion, indicating that some amount of an amorphous phase must have formed. XRPD measurements of the solidified melt prove that modification **I** has formed exclusively (Figure S3 in

the ESI). When the residue was heated in a second DSC run the same heat of fusion as in the first DSC run is observed, which clearly shows that the amorphous content crystallizes into form **I** without any detectable heat flow (Figure 5). Additional DSC measurements at different heating and cooling rates show no differences and the residues after cooling always consist of form **I** exclusively (Figure S4 in the ESI).

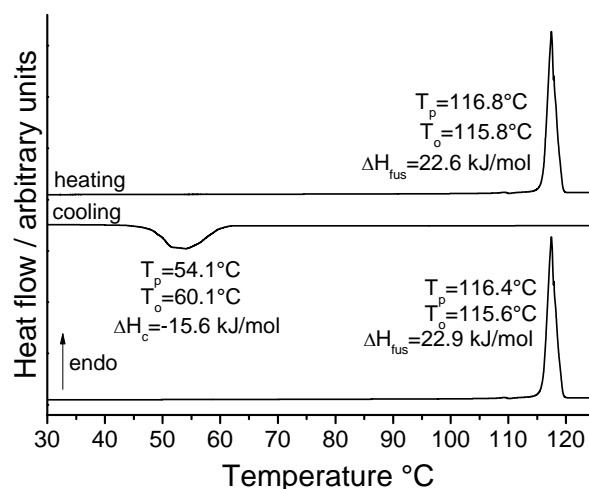


Figure 5. DSC Heating and cooling curves of form **I** performed at $3^\circ\text{C}/\text{min}$. Given are the enthalpies (heat of fusion ΔH_{fus} and heat of crystallization ΔH_c) as well as the peak (T_p) and onset (T_o) temperatures.

During quick cooling (at $20^\circ\text{C}/\text{min}$) no solidification can be observed indicating that a complete transformation into an amorphous phase has taken place (Figure S5 in the ESI). On further heating an exothermic peak can be observed at $T_o = 59.5^\circ\text{C}$ that can be assigned to the crystallization of the amorphous phase (Figure S5 in the ESI). In some of these measurements a small endothermic peak is observed before melting, indicating that an additional modification is obtained during crystallization which transforms into form **I** when heated.

However, this observation is not completely reproducible. XRPD measurements on the solid obtained during the quick cooling process show that the sample crystallizes immediately during sample preparation, which clearly proves that the amorphous phase is extremely unstable. In some of the powder patterns there are strong indications that a small amount of form **II** is present, which could explain the endothermic signal observed before melting. However, in several measurements always slightly different results are obtained, which is not surprising because several parameters like, e.g., the crystallization kinetics or the presence of nuclei of a given form determine which crystalline phases forms during crystallization.^[26-29]

The investigations presented above show that form **I** is the thermodynamically stable one at room-temperature and that therefore, form **II** and form **III** are metastable and were accidentally obtained by kinetic control. Therefore, we tried to obtain one of these forms by fast crystallization. In these experiments the compound was dissolved in ethyl acetate and the solvent was rapidly removed at different temperatures. A comparison of the experimental powder pattern of the residues with the calculated ones from single crystal data shows that a

Cite this: DOI: 10.1039/c0xx00000x

www.rsc.org/xxxxxx

mixture of form **I** and **II** is obtained with form **II** as the minor crystalline phase (Figure 6). Under different experimental conditions either similar mixtures of both forms could be obtained or modification **I** formed exclusively. Unfortunately, in none of these experiments phase pure samples of form **II** could be obtained.

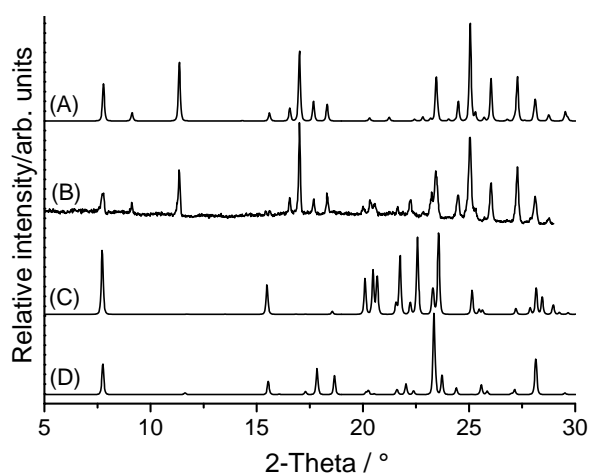


Figure 6. Experimental X-ray powder pattern of the material obtained by fast crystallization (B) and calculated powder pattern for form **I** (A), **II** (C) and **III** (D).

To investigate the transition behavior of form **II**, the mixture of **I** and **II** was investigated by means of DSC measurements. During the heating process two endothermic events have been observed. The second one corresponds to the melting point of form **I** (Figure 7). The first endothermic peak at $T_o=106.4$ °C is very broad and less intense which hints at a polymorphic transformation. If in a second DSC run the sample is cooled down after this transition, cooled down and reheated again, this endothermic signal is absent, which shows that this event is irreversible within the time scale of the experiment. XRPD measurements on the residue formed in the first endothermic transition prove that form **II** has been transformed into form **I** (Figure S6 in the ESI).

If one assume that this endothermic transition of **II** into **I** proceeds *via* the solid state, according to the heat of transition rule both forms shall be enantiotropically related and form **II** shall become more stable at lower temperatures.^[30] In this case our observation is in contradiction with the so-called density rule because form **I** is more dense than form **II**.^[31] However, the differences in density are rather small and several exceptions from this rule are known, especially when hydrogen bonding is involved, which is the case in all modifications.^[32-34]

The endothermic signal before melting of form **I** can also originate from melting of form **II** and in this case all considerations made above are not valid. Therefore heating rate-dependent measurements were performed using different

batches. A small exothermic peak would be expected after melting at very low heating rates which would correspond to the crystallization of form **I**. Such a successive endo-exo-endo transition can be observed, e.g., if a metastable form melts and a new modification with a higher melting point crystallizes from the melt.^[27] Depending on the investigated batch we obtained slightly different results. In some of these measurements the endothermic event occurs at higher heating rates and is absent for lower heating rates, which is not expected if this event corresponds to the melting of a metastable form (Figure S7 in the ESI). This observation agrees more with a solid to solid polymorphic phase transition where this transition proceeds over a large temperature range during slow heating and in this case is not detectable in the DSC measurements. Faster DSC measurements give also no evidence that this transition can be suppressed. Therefore the melting point of form **II** is still unknown (Figure S7 in the ESI). Moreover, on fast heating the melting peak becomes broader, which indicates that a further process is involved at this temperature but this cannot be resolved.

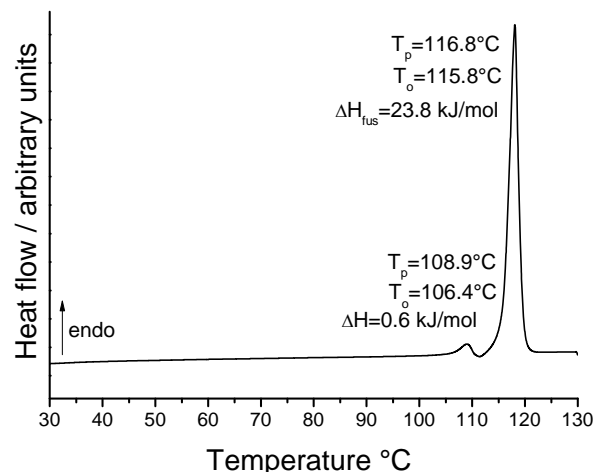


Figure 7. DSC curve of a mixture of form **I** and **II** with form **I** as the major phase. The enthalpies are given in kJ/mol and the peak (T_p) and onset (T_o) temperatures in °C.

All investigations described above indicate that form **II** should become more stable at lower temperature, therefore a saturated solution of the compound with an excess of a mixture of **I** and **II** was stored in a refrigerator at -20 °C for more than one week. XRPD investigations of the residue prove that even at this temperature form **I** is obtained exclusively (Figure S8 in the ESI). Therefore, the exact thermodynamic transition temperature must be lower.

In all experiments mentioned above we have found no access to phase-pure samples of form **II** or form **III**. In this context it has

to be noted that a metastable modification might also be prepared by solvent removal from solvates. To investigate the formation of solvates, a saturated solution of form **I** with an excess of solid was stirred in different solvents for more than one week. Afterwards the residues were characterized by X-ray powder diffraction. Unfortunately, all of the residues consist only of form **I** and therefore no solvates are accessible (Figure S9 in the ESI).

We also tried to prepare one of the metastable forms by sublimation. In this case an amorphous residue is obtained that immediately crystallizes into form **I** due to mechanic stress (Figure S10 in the ESI). Finally, when a saturated solution of this compound in ethanol is mixed with n-hexane and the precipitate is immediately filtered off and characterized by XRPD, form **I** is obtained exclusively (Figure S11 in the ESI). In summary we have found no access to larger amounts or pure samples of one of the metastable forms.

As mentioned in the beginning crystals of form **II** and **III** were accidentally obtained by crystallization from ethyl acetate and some of them were stored in inert oil. Under these conditions the crystals do not transform into form **I** and we could use them for thermomicroscopic investigations. When a single crystal of form **I** was heated at 3°C/min melting was observed at about 122.5°C (Figure S12 in the ESI). The difference in the melting temperature compared to that determined by DSC can be traced back to the imprecise calibration of the hot-stage, which is unimportant in this case. As expected there are no hints for any polymorphic transition before melting. In a similar measurement performed on form **II** between 105 and 113°C the crystals became full of cracks (Figure S13 in the ESI). During this transformation small needle-like crystals grow on the surface of the crystal, which is typical for a reconstructive polymorphic transition that proceeds *via* nucleation and grow of a new crystalline phase. This observation strongly indicates that the small endothermic signal observed in the DSC run shown in Figure 6 corresponds to a solid-to-solid polymorphic transition and not to the melting of form **II**. On further heating melting of the modification that formed during the transition is observed at about 120°C. Thermomicroscopic measurements on form **III** also show a polymorphic transition that occurs between 94.5 and 99.5°C and melting is observed at about 119.5°C (Figure S14 in the ESI).

To compare the melting temperatures more precisely the crystals of all three forms were investigated simultaneously, which proves that form **II** and form **III** transform into new modifications which melt at the same temperature (Figure S15 and S16 in the ESI). This measurement indicates that the melting point of the two modification formed by the polymorphic transition is significantly lower than that of form **I**, which would be in contradiction to some conclusions mentioned above. In this context one has to keep in mind that during the reconstructive polymorphic transition a microcrystalline powder is obtained. Under this relatively fast heating rate the melting point can be lower compared to the compact crystals of form **I**. Therefore a final measurement with a heating rate of 0.1°C/min was performed which shows that within the experimental uncertainty all samples melt at the same temperature (Figure 8).

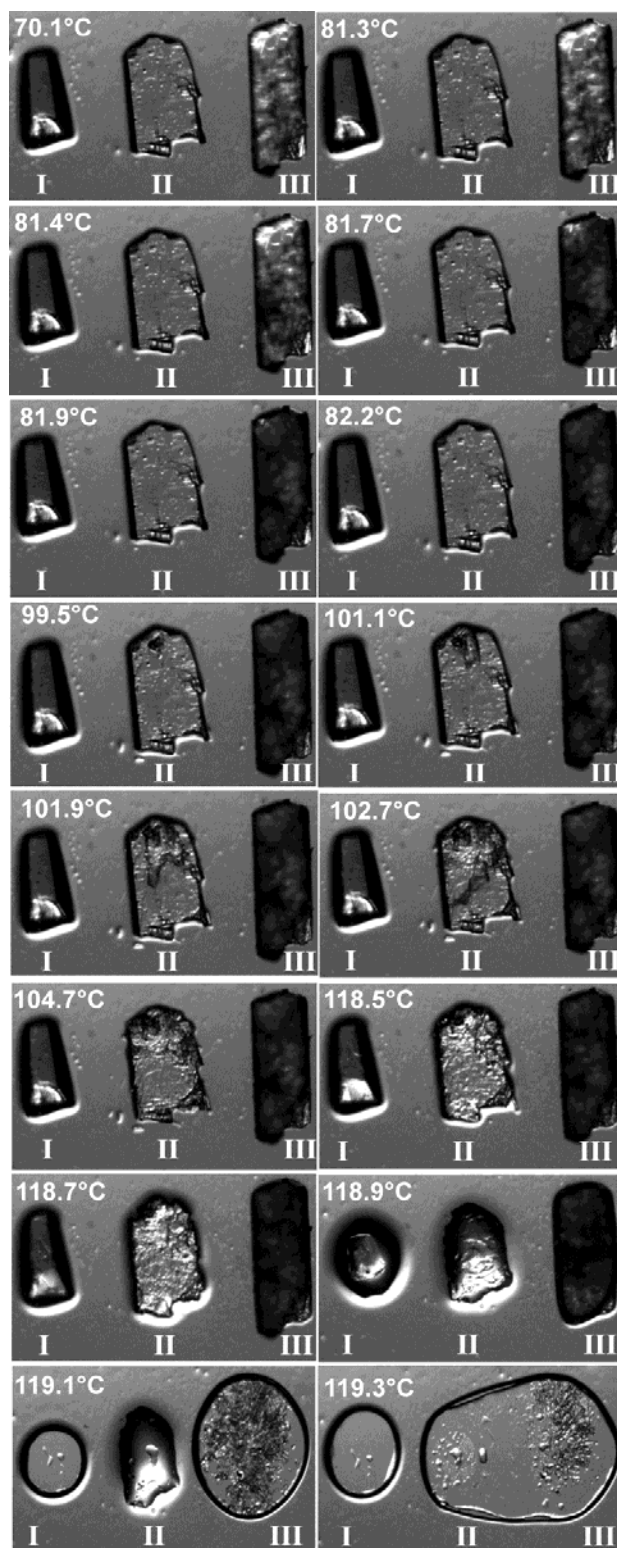


Figure 8. Selected microscopic images as a function of temperature at 0.1°C/min of form **I**, **II** and **III**.

Conclusions

In the present contribution three polymorphic modifications of *N*-(3-pyridyl)-benzamide are presented that show significant differences in the conformation of the molecules, in the nature of hydrogen bonding and in the packing of the molecules in the crystal. Quantum chemical calculations reveal, that the conformation observed in one of the two molecules in form **II** is energetically favored but this form does not correspond to

Cite this: DOI: 10.1039/c0xx00000x

www.rsc.org/xxxxxx

the energy minimum. We have found that form **I** in which the molecules are linked by N-H...N hydrogen bonding into chains represents the thermodynamic stable form at room temperature. This form should also be stable until the melting point. Even though large effort have been made we have not found access to phase-pure samples of one of the metastable forms **II** and **III** and therefore, the thermodynamic relations were not completely elucidated. We have strong hints that form **I** is enantiotropically related to form **II** and that form **II** becomes thermodynamically stable at lower temperatures. Our investigations also indicate that form **III** transforms into form **I** but this has not been fully proven because we do not know the direction of heat flow. The thermodynamical relations between **I** and **III** are therefore still unknown. The fact that a metastable form is accidentally obtained is quite usual and several examples are reported in literature. It is also well known that the preparation of such a form as a pure phase or even as mixture is extremely difficult in the presence of the stable form and this is despite the large effort we have made exactly what we have found in our investigations.

Experimental Section

Syntheses

A mixture of 12.2 g (100 mmol) benzoic acid and 9.41 g (100 mmol) 3-aminopyridine was stirred for 5 h at 160 °C. After adding 50 ml H₂O and 50 ml saturated NaHCO₃ the crude product precipitated as a brown solid which was purified by column chromatography (*R_f* = 0.33, ethyl acetate). The reaction yielded 2.75 g (14 mmol, 14 %) of a crystalline solid. ¹H NMR (500 MHz, 300 K, DMSO-d₆): δ = 10.44 (s, 1H, NH), 8.94 (d, ³*J* = 2.5 Hz, 1H), 8.32 (dd, ³*J* = 4.7 Hz, ⁴*J* = 1.5 Hz, 1H), 8.20 (ddd, ³*J* = 8.3 Hz, ⁴*J* = 2.5, ⁴*J* = 1.5 Hz, 1H), 7.98 (m, 2H), 7.62 (ddd, ³*J* = 6.6 Hz, ⁴*J* = 4.5, ⁴*J* = 1.3 Hz, 1H), 7.56 (m, 2H), 7.40 (ddd, ³*J* = 8.3 Hz, ⁴*J* = 4.7, ⁴*J* = 0.7 Hz, 1H) ppm.

Single-crystal structure analysis

Single-crystal data collections were carried out using an imaging plate diffraction system: Stoe IPDS-1 for **II** and **III** and Stoe IPDS-2 for **I** with MoK α radiation. The structures were solved with Direct Methods using SHELXS-97 and structure refinements were performed against F₂ using SHELXL-97.^[35] All non-hydrogen atoms were refined with anisotropic displacement parameters. All hydrogen atoms were located in difference map and were refined with varying coordinates and varying displacement parameters to be sure that all atoms were correctly assigned. In the final refinement the H atoms were positioned with idealized geometry and were refined isotropically with *U*_{iso}(H) = -1.2 *U*_{eq}(C) using a riding model. Because no strong anomalous scattering atoms are present the absolute structure of form **II** cannot be determined. Therefore, Friedel opposites were merged in the refinement leading to a low data to parameter ratio. All crystals of form **II** contain a small amount of a second individual but the

reflections of both of them cannot be indexed separately. Moreover, because the angle β is close to 90° the crystal is additionally pseudo-merohedrally twinned with a mirror plane as the twin element. Therefore, a twin refinement was performed leading to a value of the BASF parameter of 0.041 (2). Selected crystal data and details on the structure determinations can be found in Table 4.

It is noted that the crystal structure of form **I** and form **III** was additionally determined at room temperature to check if large differences occur in the positions of the reflections of their x-ray powder patterns, which is not the case. All geometrical parameters given in this paper originated from the low temperature study.

Table 4. Crystal data and results of the structure refinement for form **I**, **II** and **III**.

Form	I	II	III
Formula	C ₁₂ H ₁₀ N ₂ O	C ₁₂ H ₁₀ N ₂ O	C ₁₂ H ₁₀ N ₂ O
MW / g mol ⁻¹	198.22	198.22	198.22
Crystal system	monoclinic	monoclinic	monoclinic
Space group	P2 ₁ /c	P2 ₁	C2/c
<i>a</i> / Å	3.9459(2)	5.2575(6)	24.078(2)
<i>b</i> / Å	22.7301(8)	22.8695(16)	5.2381(2)
<i>c</i> / Å	11.1951(5)	7.9917(9)	15.9279(13)
β / °	107.725(4)	90.610(13)	109.382(9)
<i>V</i> / Å ³	956.43(7)	960.84(17)	1895.0(2)
<i>T</i> / K	200	200	200
<i>Z</i>	4	4	8
<i>D</i> _{calc} / g cm ⁻³	1.377	1.370	1.390
μ / mm ⁻¹	0.090	0.090	0.090
Scan range / °	1.70-27.33	2.55-25.00	2.71-26.85
Measured reflections	14064	6380	8132
Unique reflections	2138	1736	2042
Refl. [<i>F</i> ₀ > 4 σ (<i>F</i> ₀)]	1828	1538	1568
<i>R</i> _{int}	0.0556	0.0689	0.0596
Parameters	137	273	137
<i>R</i> ₁ ^a [<i>F</i> ₀ > 4 σ (<i>F</i> ₀)]	0.0419	0.0585	0.0465
<i>wR</i> ₂ ^b [all data]	0.1101	0.1591	0.1214
GOF	1.048	1.110	1.030
$\Delta\rho_{\max}/\Delta\rho_{\min}$ / e Å ⁻³	0.199/-0.122	0.319/-0.262	0.265/-0.312

CCDC 989630 (Form **I** at 200K), CCDC 989631 (Form **I** at 293K), CCDC 989632 (Form **II** at 200 K), CCDC 989633 (Form **III** at 200 K) and CCDC 989634 (Form **III** at 293K),

contain the supplementary crystallographic data for this paper. These data can be obtained free charge from the Cambridge Crystallographic Data Centre via http://www.ccdc.cam.ac.uk/data_request/cif.

Differential Scanning Calorimetry

The DSC experiments were performed using a DSC 1 Star System with STARE Excellence Software from Mettler-Toledo AG. The instrument was calibrated using standard reference materials. Several measurements using different heating and cooling rates were performed in closed Al pans.

X-Ray Powder Diffraction (XRPD)

The measurements were performed using 1) a PANalytical X'Pert Pro MPD Reflection Powder Diffraction System with CuK α radiation ($\lambda = 154.0598$ pm) equipped with a PIXcel semiconductor detector from PANalytical and 2) a Stoe Transmission Powder Diffraction System (STADI P) with CuK α radiation ($\lambda = 154.0598$ pm) that was equipped with a linear position-sensitive detector from STOE & CIE.

Calculations

Quantum chemical calculations were performed by density functional theory (DFT) using Gaussian09.^[36] The structures and vibrational frequencies of the molecules in their electronic ground states were calculated at the B3LYP/6-311++G(d,p) level of theory.

Acknowledgement

This project was supported by the state of Schleswig-Holstein. We thank Prof. Dr. Wolfgang Bensch for access to his experimental facilities. The work of JB, DB and FT has been supported by the Deutsche Forschungsgemeinschaft through the Sonderforschungsbereich 677 "Function by Switching".

Notes

^{a†} Institut für Anorganische Chemie, Universität Kiel, Max-Eyth-Straße 2, D-24118 Kiel, Germany

^b Institut für Physikalische Chemie, Universität Kiel, Max-Eyth-Straße 1, D-24118 Kiel, Germany

[†]Electronic Supplementary Information available: X-ray powder pattern, DSC curves and thermomicroscopic images of different samples. This material is available free of charge via the internet at <http://pubs.acs.org>.

References

- [1] Douhal, A., Lahmani, F., Zewail, A. *Chem. Phys.* **1996**, *207*, 477–498.
- [2] Elsaesser, T., Bakker, H. J. ed., *Ultrafast hydrogen bonding dynamics and proton transfer processes in the condensed phase*, Kluwer, Dordrecht, **2002**.
- [3] Bahrenburg, J., Temps, F., Rode, M. F., Nowacki, J., Sobolewski, A. L., manuscript in preparation.
- [4] Desiraju, G. R. *Crystal Engineering: The Design of Organic Solids*, Elsevier, Amsterdam, **1989**.
- [5] Bernstein, J., Davey, R., Henck, O. *Angew. Chem. Int. Ed.* **1999**, *38*, 3440–3461.
- [6] Hilfiker, R. *Polymorphism in the Pharmaceutical Industry*, WILEY-VCH, **2006**.
- [7] Brittain, H. G. *Polymorphism in pharmaceutical Solids*, Vol. 23, Marcel Dekker Inc.: New York, **1999**.
- [8] Braga, D., Grepioni, F. *Making Crystals by Design: Methods, Techniques and Applications*, Wiley-VCH Verlag GmbH & Co. KGaA, Weinheim, **2007**.
- [9] Desiraju, G.R. *Crystal Design: Structure and Function*, ed. G. R. Desiraju, Wiley, Chichester, **2003**.
- [10] McCrone, W. C. *Polymorphism in Physics and Chemistry of the Organic Solid State*, ed. D. Fox, M. M. Labes and A. Weissenberg, Interscience, New York, vol. II, pp. 726, **1965**.
- [11] Näther, C., Suitchmezian, V., Jess, I. *J. Pharm. Sci.*, **2008**, *97*, 4516–4527.
- [12] Užarević, K., Rubčić, M., Đilović, I., Kokan, Z., Matković-Čalogović, D., Cindrić, M. *Cryst. Growth Des.* **2009**, *9* (12), 5327.
- [13] Vrdoljak, V., Prugovečki, B., Matković-Čalogović, D., Hrenar, T., Dreos, R., Siega, P. *Cryst. Growth Des.* **2013**, *13* (8), 3773–3784.
- [14] Roy, S., Nangia, A., *Cryst Growth Des.* **2007**, *7* (10), 2047–2058.
- [15] Näther, C., Bhosekar, G., Jess, I. *Inorg. Chem.*, **2007**, *48*, 8079–8087.
- [16] Dean, P., Scudder, M., Craig, D., Dance, I. *CrystEngComm*. **2001**, *3*, 84–90.
- [17] Horn, C., Scudder, M., Dance, I. *CrystEngComm*. **2000**, *2*, 53–66.
- [18] Nizhnik, Y. P., Lu, J., Rosokha, S. V. *CrystEngComm*. **2009**, *11*, 2400–2405.
- [19] Stirling, C. J. M., Fundin, L. J., Williams, N. H. *Chem. Commun.* **2007**, *17*, 1748–1750.
- [20] Schödel, H., Näther, C., Bock, H. Butenschön, *Acta Cryst. B*, **1996**, *52*, 842–853.
- [21] Näther, C., Jess, I., Havlas, Z., Nagel, N., Bolte, M., Nick, S., *Solid State Sci.*, **2002**, *4*(6), 859–871.
- [22] Wriedt, M., Yakovenko, A. A., Haider, G. J., Prosvirin, A. V., Dunbar, K., Zhou, H. C. *J. Am. Chem. Soc.* **2013**, *135*, 4040–4050.
- [23] Malla Reddy, C.; Basavoju, S.; Desiraju, G. R.; *Chem. Commun.*, **2005**, 2439–2441
- [24] Bhattacharya, S.; Saha, B. K. *Cryst.GrowthDes.* **2013**, *13*, 606–613.
- [25] Cruz-Cabeza, A. J., Bernstein, J. *Chem. Rev.* **2013**, doi.org/10.1021/cr400249d
- [26] Dunitz, J. D., Bernstein, J. *Acc. Chem. Res.*, **1995**, *28*(4), 193–200.
- [27] Näther, C., Jess, I., Jones, P. G., Taouss, C., Teschmit, N. *Cryst.Growth Des.*, **2013**, *13*, 1676–1684.
- [28] Mnyukh, Y. V. *Molecular Crystals and Liquid Crystals*, **1979**, *52*, 201–217.
- [29] Kishi, Y., Matsuoka, M. *Cryst. Growth Des.* **2010**, *10*, 2916–2920.
- [30] Burger, R., Ramberger, R. *Mikrochim. Acta*, **1979**, *2*, 274–316.
- [31] Kitaigorodskii, A. I. *Molecular Crystals and Molecules*, Academic Press, New York, **1973**.
- [32] Robertson, J. M., Ubbelohde, A. R. *Proc. Royal Soc. London Ser. A*. **1938**, *167*, 136–147.
- [33] Griesser, U. J., Burger, A., Mereiter, K. *J. Pharm. Sci.* **1995**, *86*, 352–358.
- [34] Haisa, M., Kashino, S., Maeda, H. *Acta Cryst.B*, **1974**, *30*, 2510–2512.
- [35] Sheldrick, G. M. *Acta Cryst. A*, **2008**, *64*, 112–122.
- [36] Frisch, M. J., Trucks, G. W., Schlegel, H. B., Scuseria, G. E., Robb, M. A., Cheeseman, J. R., Scalmani, G., Barone, V., Mennucci, B., Petersson, G. A., Nakatsuji, H., Caricato, M., Li, X., Hratchian, H. P., Izmaylov, A. F., Bloino, J., Zheng, G., Sonnenberg, J. L., Hada, M., Ehara, M., Toyota, K., Fukuda, R., Hasegawa, J., Ishida, M., Nakajima, T., Honda, Y., Kitao, O., Nakai, H., Vreven, T., Montgomery, J. A., Jr., Peralta, J. E., Ogliaro, F., Bearpark, M., Heyd, J. J., Brothers, E., Kudin, K. N., Staroverov, V. N., Kobayashi, R., Normand, J., Raghavachari, K., Rendell, A., Burant, J. C., Iyengar, S. S., Tomasi, J., Cossi, M., Rega, N., Millam, N. J., Klene, M., Knox, J. E., Cross, J. B., Bakken, V., Adamo, C., Jaramillo, J., Gomperts, R., Stratmann, R. E., Yazyev, O., Austin, A. J., Cammi, R., Pomelli, C., Ochterski, J. W., Martin, R. L., Morokuma, K., Zakrzewski, V. G., Voth, G. A., Salvador, P., Dannenberg, J. J., Dapprich, S., Daniels, A. D., Farkas, Ö., Foresman, J. B., Ortiz, J. V., Cioslowski, J., Fox, D. J. *GAUSSIAN09* (Revision A.02), Gaussian Inc., Wallingford, CT, U.S.A., 2009.

Cite this: DOI: 10.1039/c0xx00000x

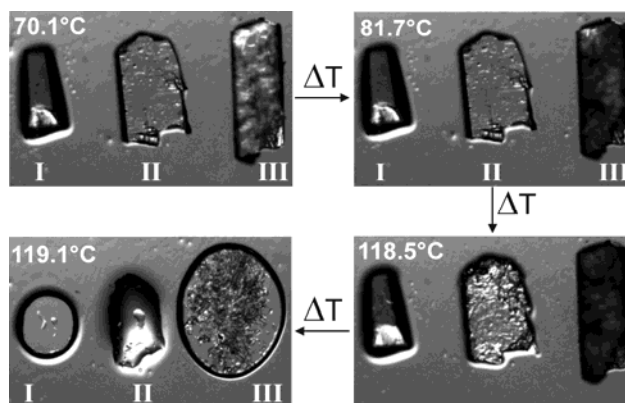
www.rsc.org/xxxxxx

PAPER

Figure for the table of contents

Investigations on the Trimorphism of *N*-(3-pyridyl)-benzamide

Christian Näther, Inke Jess, Julia Bahrenburg, Dennis Bank and Friedrich Temps



Three polymorphic modifications of *N*-(3-pyridyl)-benzamide were structurally characterized and investigated for their transition behavior and thermodynamic relations.